INTERNATIONAL JOURNAL FOR NUMERICAL METHODS IN FLUIDS
Int. J. Numer. Meth. Fluids 2008; **56**:1271–1280
Published online in Wiley InterScience (www.interscience.wiley.com). DOI: 10.1002/fld.1741

Large-eddy simulation of the flow in a low-speed centrifugal compressor

K. M. Guleren[1,*,†], A. Turan[2] and A. Pinarbasi[1]

[1]*Mechanical Engineering Department, Faculty of Engineering, Cumhuriyet University, 58140 Sivas, Turkey*
[2]*School of Mechanical, Aerospace and Civil Engineering, University of Manchester, M60 1QD Manchester, U.K.*

SUMMARY

The results of a series of numerical simulations for the NASA low-speed centrifugal compressor are presented. Large-eddy simulation (LES) is carried out together with the most commonly used Reynolds-averaged Navier–Stokes (RANS) models, including the mixing length, k–ε and k–ω models. Predictions are compared with the available experimental data. It is seen that quantitative predictions of LES are better than those of RANS models for the tip jet and wake regions. LES, unlike these RANS models and the past computational fluid dynamics predictions, shows separation near the casing starting around the halfway of the impeller and reveals a vortex bubble close the impeller exit/casing corner. The tip leakage flow, which is the main characteristic of an unshrouded compressor, is investigated using the probability density function (PDF) and the power spectral density (PSD) of the instantaneous velocity values. The skewness and flatness calculated from the PDF profiles show that the unsteady flow in the tip wake region is less-intermittent compared with the flow in the tip jet region. The PSD analysis shows that the turbulent energy transfer rate from the larger scales to the smaller scales and the frequency range where the inertial region is valid increase in the tip wake region.

Received 13 April 2007; Revised 27 November 2007; Accepted 4 December 2007

KEY WORDS: LES; RANS; centrifugal compressor; separation; tip leakage; probability density function; power spectral density

1. INTRODUCTION

Numerous experimental and numerical studies have provided valuable insights regarding the understanding of the basic flow physics in the centrifugal turbomachinery. Eckardt [1] revealed the first evidence of a 'jet-wake' flow phenomenon. The jet-flow, seen at the exit of the impeller, was observed to comprise two parts: a low-momentum region near the suction surface/shroud corner with high turbulence values and losses and a jet region characterized by a

*Correspondence to: K. M. Guleren, Mechanical Engineering Department, Faculty of Engineering, Cumhuriyet University, 58140 Sivas, Turkey.
†E-mail: melihguleren@cumhuriyet.edu.tr

high tangential velocity component near the pressure side with a relatively stable flow and low pressure losses. Hathaway *et al*. [2] and Zhang *et al*. [3] simulated the flow in an unshrouded compressor and failed to predict the size and the origin of the wake with Reynolds-averaged Navier–Stokes (RANS) models accurately. Recently, large-eddy simulation (LES) has been employed as an alternative research tool for turbomachinery flows. Song and Chen [4] and Chen *et al*. [5] performed LES of a Francis turbine to investigate the unsteady nature of the flow and to model the turbine system based on LES predictions. Kato *et al*. [6] and Byskov *et al*. [7] presented the first (or perhaps earliest) successful predictions using LES for the complex flow in a mixed flow and a centrifugal pump, respectively. Jang *et al*. [8] investigated the vortical flow field in a propeller fan with special emphasis on tip and leading-edge vortex structures.

2. FLOW CASE AND NUMERICAL ASPECTS

LES is a numerical technique used for solving transient and turbulent flows. It is based on resolving the larger flow scales and modelling the smaller ones. The former characterize most of the energetic structures and are problem dependent, whereas the latter are assumed to be universal [9]. In order to account for the large-scale behaviour considering the modelled small scales, a filtering operation is performed. The filtered continuity and Navier–Stokes equations for rotating and incompressible flows read as

$$\frac{\partial \bar{u}_i}{\partial x_i} = 0 \tag{1}$$

$$\frac{\partial \bar{u}_i}{\partial t} + \frac{(\partial \bar{u}_i \bar{u}_j)}{\partial x_j} = -\frac{1}{\rho}\frac{\partial \bar{P}}{\partial x_i} + \frac{\partial}{\partial x_j}\left(\nu \frac{\partial \bar{u}_i \bar{u}_j}{\partial x_j}\right) - \frac{\partial \tau_{ij}^{\mathrm{sgs}}}{\partial x_j} + \varepsilon_{ij3} 2\Omega \bar{u}_j \tag{2}$$

where ε_{ij3} is the Levi–Civita's alternating tensor. The last term of Equation (2) is the Coriolis force. The centrifugal force is combined with the pressure resulting in the modified pressure $\bar{P}$. τ_{ij}^{sgs} represents the subgrid-scale (SGS) stresses modelled based on Bousinesq approach, i.e.

$$\tau_{ij}^{\mathrm{sgs}} - \tfrac{1}{3}\delta_{ij}\tau_{kk}^{\mathrm{sgs}} = -2\nu_t \bar{S}_{ij} \tag{3}$$

where δ_{ij} is the Kronecker delta, $\bar{S}_{ij}$ is the resolved-scale strain rate tensor, and ν_t is the SGS eddy viscosity. The resolved-scale strain rate tensor is defined as

$$\bar{S}_{ij} \equiv \frac{1}{2}\left(\frac{\partial \bar{u}_i}{\partial x_j} + \frac{\partial \bar{u}_j}{\partial x_i}\right) \tag{4}$$

In this study, the SGS stresses are modelled using the wall-adapting local eddy-viscosity (WALE) model [10]. This model takes into account both the effects of strain and rotation rates. The SGS eddy viscosity for the WALE model is defined as

$$\nu_t = (C_w \Delta)^2 \frac{(S_{ij}^d S_{ij}^d)^{3/2}}{(\bar{S}_{ij}\bar{S}_{ij})^{5/2} + (S_{ij}^d S_{ij}^d)^{5/4}} \tag{5}$$

DOI: 10.1002/fld

where

$$S_{ij}^{d}=\frac{1}{2}(\bar{g}_{ij}^{2}+\bar{g}_{ji}^{2})-\frac{1}{3}\delta_{ij}\bar{g}_{kk}^{2} \quad \text{and} \quad \bar{g}_{ij}=\frac{\partial \bar{u}_i}{\partial x_j} \tag{6}$$

Here Δ is the cube root of the cell volume ($\Delta=V_{\text{cell}}^{1/3}$) and the model coefficient is $C_w=0.1$. $\bar{g}_{ij}$ represents the resolved-scale velocity gradient and is of the order of resolved-scale strain rate tensor. The SGS eddy viscosity defined in Equation (5) drops naturally to zero near the walls. This provides the correct near-wall behaviour unlike the Smagorinsky model [11]. Therefore, the WALE model can be considered as an alternative model to the Smagorinsky model. Further information and the justification of this model can be found in [12].

Flow calculations are performed using a multi-purpose flow solver [13]. The governing integral equations for the conservation of mass and momentum are solved via a finite-volume technique based on the projection method. A pressure-correction equation is solved to obtain the corrected velocity and pressure fields and mass fluxes so that continuity is satisfied. The set of linearized equations are solved by the Gauss–Seidel method, which is coupled with an algebraic multigrid method to accelerate convergence. A bounded central differencing scheme is used for the convection term. A fully second-order implicit scheme is applied for temporal discretization. The PISO algorithm and the PRESTO! scheme are adopted for the velocity–pressure coupling and pressure interpolation, respectively. Details of the implementation of LES and RANS and related numerics for the current problem can be found in [14].

Low-speed centrifugal compressors (LSCCs) are more suitable for the current established LES methodologies than their high-speed counterparts considering the Reynolds number and compressibility effects. Moore and Moore [15] calculated the relative Mach number to be less than 0.3 for the NASA LSCC. Considering this, the variation in density becomes negligibly small. This justifies the use of an 'incompressible' flow assumption for the modelling of the flow in LSCC. Furthermore, concerns regarding the SGS modelling and boundary conditions are eliminated. The LSCC was designed by NASA engineers to duplicate the essential flow physics in a high-speed subsonic centrifugal compressor [2]. The LSCC is composed of 20 full impeller blades with a 55° backsweep-angle. The design tip speed is 153 m/s. The inlet and the exit diameters of the impeller are 87 and 152.4 cm, respectively. Corresponding widths of the impeller blades at the inlet and the exit are 21.8 and 14.1 cm, respectively. The LSCC flow field had a design mass flow rate of 30 kg/s and a rotational speed of 1862 rpm.

In this study, the multiple reference frame (MRF) [16] is used. In the MRF model, the computational domain is divided into sub-domains and each domain is defined as stationary or rotating with respect to the inertial frame. The LSCC is divided into three sub-domains: upstream of the impeller ($-0.38<m_i/m<0$) as stationary, impeller ($0<m_i/m<1$) as rotating and the diffuser ($1<m_i/m<2$) as stationary, where m is the total meridional distance of the impeller and m_i is the meridional distance from the impeller inlet. At the inlet ($m_i/m=-0.38$), available experimental measurements of velocities are interpolated to the computational grid. Turbulent parameters for RANS and LES are described in detail in [14]. The impeller blades and the attached hub surface are assumed to be rotating with the rotational speed of $\Omega=1862$ rpm. No-slip boundary condition is applied for the other wall boundaries. Periodic boundary conditions are used at the mid-pitch of the pressure side (PS) and suction side (SS) of the blades. The periodic boundaries are extended towards the upstream of the impeller and the diffuser by following the blade inlet and exit angles, respectively. At the exit the outflow boundary condition is assumed, resulting in a zero-diffusion

DOI: 10.1002/fld

flux for all flow variables and in an overall mass balance correction. Three grid topologies, namely the coarse mesh (CM), the medium mesh (MM) and the fine mesh (FM), are adopted in this study to delineate the grid dependency. The computational mesh consists of $457\times44\times40$ grid cells for the CM, $756\times88\times80$ grid cells for the MM and $1111\times136\times150$ grid cells for the FM in the streamwise, spanwise and pitchwise (blade-to-blade) directions. The details of the grid distribution are shown in Table I. The adequacy of a grid resolution for LES is generally determined in terms of the grid spacing in wall units. For complex geometries, including the centrifugal compressor, the streamwise, spanwise and pitchwise directions can be defined in several ways, and each definition will yield different results for the grid spacing in wall units. Therefore, we propose another way to determine the grid resolution that could be adopted by the LES users for the complex geometries. For all grid topologies, the larger scales ($L=k^{3/2}/\varepsilon$), the Taylor length scales ($\lambda=(10\nu k/\varepsilon)^{1/2}$) and the Kolmogorov length scales ($\eta=(\nu^3/\varepsilon)^{1/4}$) are calculated as area-averaged values on meridional stations and compared with the filter length ($\Delta=V^{1/3}$). As shown in Figure 1, the CM lies between the larger and the Taylor scales, but much closer to Taylor scales. In the context of LES, the CM seems to be acceptable. However, the adopted grid resolution should be at least a Taylor-scale resolution for the investigation of the refined flow physics. This resolution level is achieved with the MM apart from the blade-wake region ($1<m_i/m<1.1$). The FM provides much better resolution since it is even smaller than the Taylor scales everywhere. The time step

Table I. Grid distribution for the LSCC.

	Streamwise			Spanwise			
	Upstream	Impeller	Diffuser	Tip	Blade	Pitchwise	Total (10^6)
CM	50	284	123	4	40	40	0.9
MM	100	512	144	8	80	80	7
FM	120	791	200	16	120	150	26

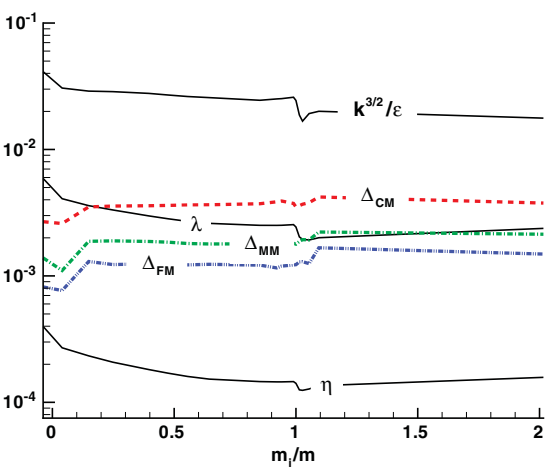

Figure 1. Spatial resolution of grid topologies.

DOI: 10.1002/fld

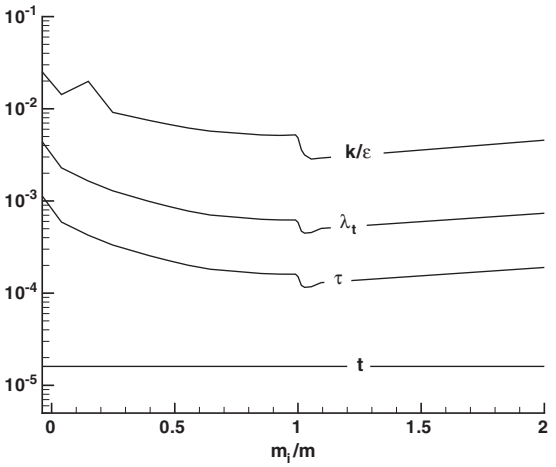

Figure 2. Temporal resolution of grid topologies.

is chosen is such a way that one blade passing is completed in 100 time steps. This corresponds to 2000 time steps to complete one full impeller revolution. Since $\Omega = 1862$ rpm, one revolution is completed in 3.2×10^{-2} s. The time step employed for the predictions is, therefore, 1.6×10^{-5} s. To find out whether the adopted time scale is small enough for LES, time scales associated with larger scales ($T = k/\varepsilon$), the Taylor time scales ($\lambda_t = (15\nu/\varepsilon)^{1/2}$) and the Kolmogorov time scales ($\tau = (\nu/\varepsilon)^{1/2}$) are calculated in a similar way of calculating length scales and compared with the adopted physical time step t. As shown in Figure 2, the physical time step is even smaller than the Kolmogorov time scales.

3. RESULTS AND DISCUSSION

For the FM resolution, y^+ values on the walls are kept to be less than 5 to be able to resolve the viscous sub-layer. However, this resolution is achieved locally for the CM and MM cases [14]. Therefore, the CM and MM cases are more susceptible to errors that would be caused by wall functions. Figures 3 and 4 show the meridional velocity distribution from the impeller inlet to the impeller exit at mid-pitch for two spanwise locations. The flow accelerates gradually starting from the impeller inlet till $m_i/m \approx 0.3$ at 50% span location and $m_i/m \approx 0.25$ till 90% span location, and then decelerates monotonically. The deceleration of the flow is often referred to as the diffusion (pressure conversion) of the flow in the turbomachinery literature. The diffusion rate of the flow is higher at 90% span than at 50% span due to the wake caused by the tip leakage flow. The results of the MM case are consistent with those of the FM case. The results of the CM case, on the other hand, display marked differences compared with the MM and FM cases, especially at 90% span location. The grid sensitivity test displayed by Figures 3 and 4 shows the mean flow results of the MM and FM cases coincide, suggesting that grid convergence is achieved at least for the meridional velocity field. The passage wake (low-velocity region) and the corresponding jet (high-velocity region) are displayed by the meridional velocity profiles in Figure 5 at $m_i/m = 0.644$. LES predicts details of both these regions better than the other models. The mixing length model performs rather

DOI: 10.1002/fld

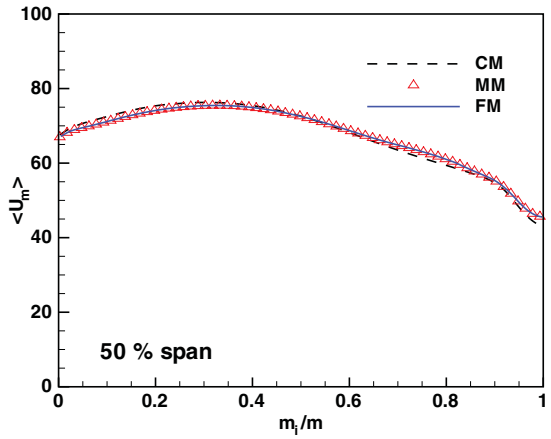

Figure 3. Meridional velocity comparisons at 50%.

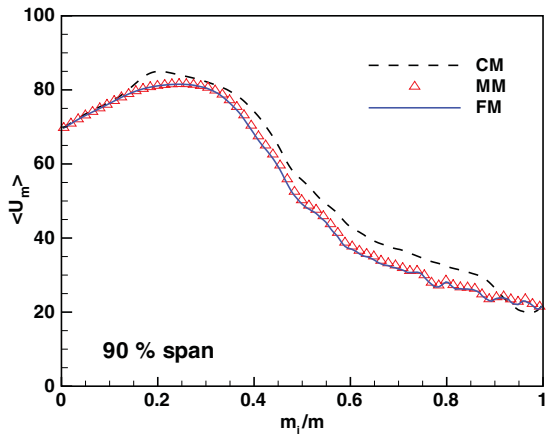

Figure 4. Meridional velocity comparisons at 90%.

disappointingly and therefore cannot be trusted for a quantitative centrifugal compressor design. The two-equation models, on the other hand, predict the wake region fairly well, but fail to capture the evolution of the corresponding tip jet flow near the SS. Figure 6 shows that LES also performs better than RANS at 50% span location, especially close to the PS and SS, where the boundary layers are significant.

In the earlier design of the LSCC, the cross-sectional area of the downstream diffuser was kept constant. However, numerical predictions of Moore and Moore [15] showed that, there was a significant separation region that originated from the impeller casing and developed through the diffuser. Based on their predictions, the diffuser was redesigned by decreasing the cross-sectional area of the diffuser. The reverse flow is an undesirable feature in the centrifugal compressor as for many turbomachinery applications. Especially for the design flow rate, the reverse flow is attributable to

DOI: 10.1002/fld

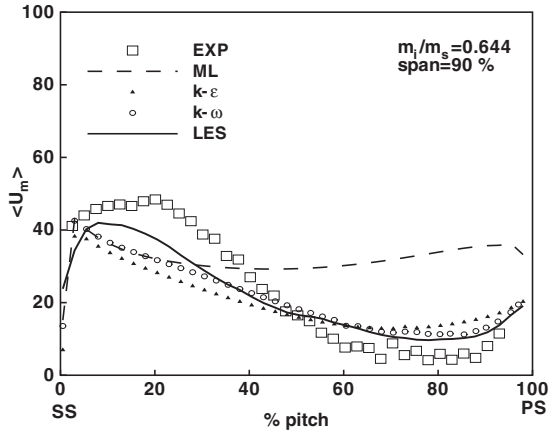

Figure 5. Blade-to-blade meridional velocity comparisons at $m_i/m = 0.644$ along 90% span.

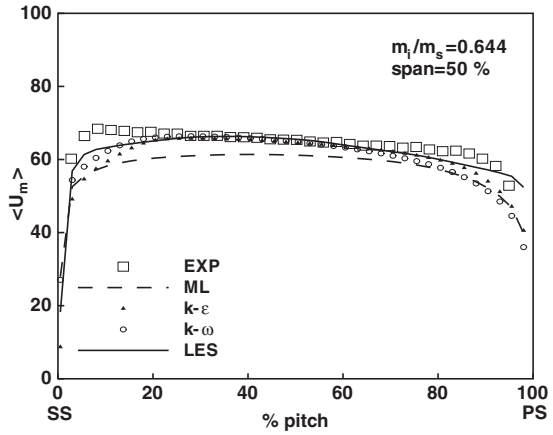

Figure 6. Blade-to-blade meridional velocity comparisons at $m_i/m = 0.644$ along 50% span.

the extremely complex flow field existing therein and hence to the limited understanding and consequently design strategies adopted for high-efficient advanced centrifugal compressors. LES, unlike RANS, provides a refined picture of the flow that would highlight additional features concerning the reverse flow behaviour. Meridional velocity contours and streamlines near the impeller exit/casing corner predicted by k–ω model and LES are shown in Figures 7 and 8, respectively. As seen in these figures, k–ω model predict neither the reverse flow nor any vortex bubble. LES, on the other hand, predicts a significant separation region which starts around the halfway of the impeller [14]. The separated region develops gradually and finally a vortex bubble is formed close to the impeller exit. Considering the LES predictions, this bubble is approximately 3.5 cm long and 0.9 cm wide which corresponds to 25 and 6.5% of the width of the blade at the exit.

Temporal history of the instantaneous velocity field is also extremely important in the context of turbulence. At station $m_i/m = 0.644$ where the jet and the wake are significantly apparent, seven

DOI: 10.1002/fld

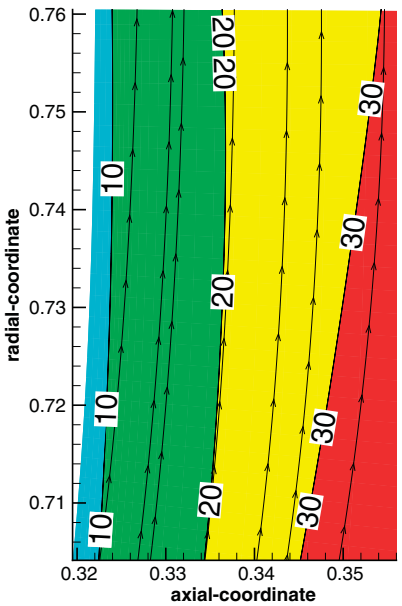

Figure 7. Meridional velocity contours and streamlines predicted by k–ω model.

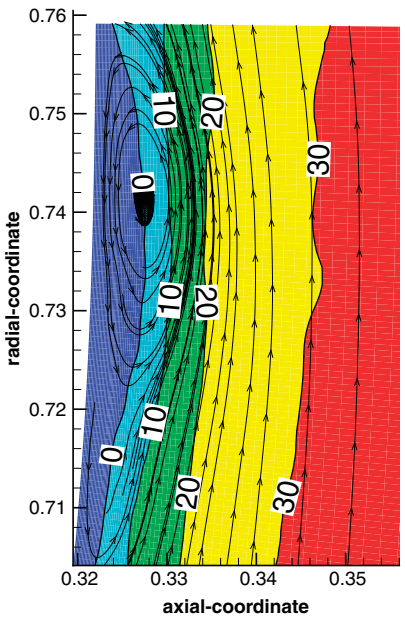

Figure 8. Time-averaged meridional velocity contours and streamlines predicted by LES.

DOI: 10.1002/fld

Table II. Skewness and flatness of the instantaneous meridional velocity.

	a	*b*	*c*	*d*	*e*	*f*	*g*	*h*	*i*
Skewness	−0.45	0.07	0.56	0.12	0.18	0.13	−0.08	0.03	0.06
Flatness	3.24	3.06	3.00	2.69	2.55	2.63	2.56	2.84	2.88

Table III. The features of inertial subrange region.

	a	*b*	*c*	*d*	*e*	*f*	*g*	*h*	*i*
Range ($\times 10^3\,s^{-1}$)	4.0	5.7	2	4.9	4.0	4.2	4.4	4.7	5.0
Slope	−3.4	−4.6	−2.3	−1.6	−1.2	−2.0	−2.7	−3.8	−3.1

points (‘*b*’, ‘*d*’, ‘*e*’, ‘*f*’, ‘*g*’, ‘*h*’ and ‘*i*’) are located in the tip clearance from the SS to the PS. Distances between these points are equal and are approximately 15% of the pitch. For 30-blade passing periods, skewness and flatness of the instantaneous radial velocity at those points and at the points close to suction and pressure sides (‘*a*’ and ‘*c*’) are calculated and tabulated in Table II. Table II suggests that instantaneous velocity values in the wake and around the tip region are less intermittent (i.e. more peaky), whereas they are highly intermittent (i.e. flatter) within around 50% pitch from the SS. At these 8 points, the energy spectra is calculated via an fast Fourier transform algorithm incorporating a Hamming window. The range and the rate of the energy transfer process associated with the energy spectra are shown in Table III. As seen, the energy transfer rate from the larger scales to the smaller scales (the slope of the inertial subrange region) and the frequency range where the inertial subrange region is valid increase as one approaches the tip wake from the SS.

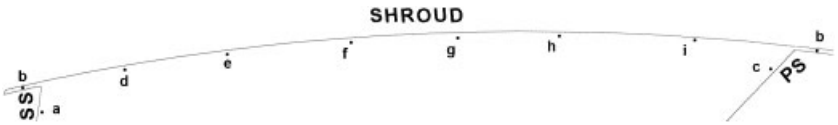

4. CONCLUSIONS

In this study, LES predictions are presented for a centrifugal compressor. Comparisons with RANS turbulence models and experimental data show that LES performs better than RANS models, especially near the tip wake and jet regions. Among the RANS models, the k–ω model is observed to perform the best. Even the k–ω model does not predict the reverse flow and the vortex bubble which are clearly captured by LES near the impeller exit/casing corner. Unsteady nature of the tip wake and jet flows is investigated via the PDF and the energy spectra of the velocity fluctuations. The PDF results suggest that the velocity values in the tip wake are less intermittent compared with the region near the SS. Spectra profiles indicate that the energy transfer rate from larger scales to smaller scales is more enhanced in the wake region.

The authors’ future activities will involve a detailed numerical study for a centrifugal impeller with a downstream vaned diffuser. The turbulence behaviour and the unsteadiness associated with

DOI: 10.1002/fld

blade passing will be tackled using LES, with the ultimate hope that advanced compressor designs can be proposed and implemented in the near future.

ACKNOWLEDGEMENTS

The authors are thankful to Dr Hathaway from the NASA Glenn Research Center for the experimental data.

REFERENCES

1. Eckardt D. Instantaneous measurements in jet-wake discharge flow of a centrifugal compressor impeller. *Journal of Engineering for Power* (ASME) 1975; **97**(3):337.
2. Hathaway MS, Chriss RM, Wood JR, Strazisar A. Experimental and computational investigation of the NASA low-speed centrifugal compressor flow field. *Journal of Turbomachinery* (ASME) 1993; **115**:527.
3. Zhang M, Pomfret MJ, Wong CM. Three-dimensional viscous flow simulation in a backswept centrifugal impeller at the design point. *Computers and Fluids* 1996; **25**(5):497.
4. Song CH, Chen X. Simulation of flow through Francis turbine by LES method. *XVIII IAHR Symposium on Hydraulic Machinery and Cavitation*, vol. 1. Dordrecht, The Netherlands, 1996; 267.
5. Chen X, Song ChCS, Tani K, Shinmei K, Niikura K, Sato J. Comprehensive modeling of Francis turbine system by large eddy simulation approach. *Hydraulic and Cavitation* 1998; **1**:236.
6. Kato C, Shimizu H, Okamura T. Large eddy simulation of unsteady flow in a mixed-flow pump. *Third ASME/JSME Joints Fluids Engineering Conference*, New York, 1999; 1.
7. Byskov RK, Jacobsen CB, Pedersen N. Flow in a centrifugal pump impeller at design and off-design conditions—Part II: large eddy simulations. *Journal of Fluids Engineering* (ASME) 2003; **125**(1):73.
8. Jang CM, Furukawa M, Inoue M. Analysis of vortical flow field in a propeller fan by LDV measurements and LES—Part I: three-dimensional vortical flow structures. *Journal of Fluids Engineering* (ASME) 2001; **123**:748.
9. Pope SB. *Turbulent Flows*. Cambridge University Press: Cambridge, 2000.
10. Nicoud F, Ducros F. Subgrid-scale stress modelling based on the square of velocity gradient tensor. *Flow Turbulence Combustion* 1999; **62**:183.
11. Smagorinsky J. General circulation experiments with primitive equations. I. The basic experiment. *Monthly Weather Review* 1963; **91**:99.
12. Guleren KM, Turan A. Validation of large-eddy simulation of strongly curved stationary and rotating U-duct flows. *International Journal of Heat and Fluid Flow* 2007; **28**:909.
13. Fluent Inc., *FLUENT 6.2 user guide*. Fluent Inc., Lebanon, U.S.A., 2001; *Computer Methods in Applied Mechanics and Engineering* 1991; **88**:17.
14. Guleren KM. Large-eddy simulation of wall-bounded flows subjected to curvature and rotation. *Ph.D. Thesis*, The University of Manchester, U.K., 2007. Available from: http://www.cumhuriyet.edu.tr/∼melihguleren/PhDthesis.pdf
15. Moore J, Moore JG. A prediction of 3-D viscous flow and performance of the NASA low-speed centrifugal compressor. *ASME Paper No. 90-GT-234*, 1990.
16. Luo JY, Issa R, Gosman AD. Prediction of impeller-induced flows in mixing vessels using multiple frames of reference. *IChemE Symposium Series* 1994; **136**:549.

DOI: 10.1002/fld